Journal of Thermal Analysis and Calorimetry (2021) 143:95–101
https://doi.org/10.1007/s10973-020-09284-9

A dynamic analysis of the aluminum titanate (Al_2TiO_5) reaction-sintering from alumina and titania, properties and effect of alumina particle size

María A. Violini[1,2] · María F. Hernández[1,2] · María S. Conconi[1,2] · Gustavo Suárez[1,2] · Nicolás M. Rendtorff[1,2]

Received: 27 February 2019 / Accepted: 3 January 2020 / Published online: 11 January 2020

Abstract
Aluminum titanate Al_2TiO_5 materials were successfully processed from different fine commercial powders and characterized. Particularly, two calcined aluminas were compared through a multitechnique approach including differential thermal analysis and dilatometry together with structural, microestructural, and mechanical characterization. This allowed the description of all the thermochemical processes during thermal treatment. Developed phases were established. Relatively dense ceramics were obtained, and complex microstructures were described with interlocked grains and an interconnected microcrack matrix that do not jeopardize the material integrity. Multistep sintering and reaction sintering processes were observed in both samples. The first stage consists of the sintering of the starting powders (alumina and titania). A second sintering stage of the starting powders was observed for both samples as well. Once advanced, the second one is overlapped with Al_2TiO_5 formation that starts at 1380 °C and finishes at 1440 °C. They affect crack development and, in consequence, the thermal behavior. The lower alumina particle size enhances the sintering and reaction advance processes. In the technological temperature range (room temperature—1000 °C), low or even negative thermal expansion behaviors were observed in the developed materials. This, together with the mechanical behavior, encourages structural applications with high thermomechanical solicitations of Al_2TiO_5 based materials.

Keywords Low thermal expansion materials · Aluminum titanate · Reaction sintering · Properties

Introduction

Aluminum titanate (Al_2TiO_5) is a material with high refractoriness and excellent thermal shock resistance. It presents a high melting point (over 1800 °C) and anisotropic thermal expansion coefficients [1–5]. Hence, it is suitable for several applications at elevated temperatures where insulation and thermal shock resistance are required [6–9], such as components of internal combustion engines, exhaust port liners, metallurgy, and thermal barriers. The thermal instability of Al_2TiO_5 is one of its disadvantages [6]. Several additives have been employed that demonstrated certain efficiency for stabilizing microstructures [6, 10–15].

The material is isomorphous with pseudobrookite, crystallizing in the orthorhombic space group Cmcm and is characterized by a pronounced anisotropy in the thermal expansion coefficient resulting in a distinct hysteresis. This anisotropy is the reason for the severe microcracking during cooling that leads to the poor mechanical properties of the sintered material. The microcracking phenomenon is closely related to the material microstructure. Below a critical grain size, the elastic energy of the system is insufficient for microcracks formation during cooling, and thus, the mechanical properties are considerably enhanced. This critical grain size depends on the thermal history of the sample and is in the range of 1–2 μm. The density of microcracks increases drastically with grain size increase once above the critical size [2, 6, 16]. The microcracking phenomenon finally determines the thermal expansion behavior of the material and the thermal diffusivity, the strength and the elastic modulus.

✉ María A. Violini
aviolini@cetmic.unlp.edu.ar

[1] Centro de Tecnología de Recursos Minerales y Cerámica CETMIC (CIC-CONICET), Cno. Centenario y 506 Gonnet, La Plata 1897, Argentina

[2] Departamento de Química, Facultad de Ciencias Exactas, UNLP, 47 y 115, La Plata 1900, Argentina

The Al_2TiO_5 formation is an endothermic process that occurs at 1280 °C [9]. Below this temperature, it is unstable and dissociates spontaneously. This represents a disadvantage for this material, so grain size and stabilizing phase incorporation have been the strategies used to overcome this tendency [6, 11].

Buscagliua et al. [17, 18] described the direct sintering process up to 1600 °C. They proposed a three-step process: the initial contraction due to the densification of the starting oxide mixture, followed by the expansion related to Al_2TiO_5 formation and a final second contraction due to AI_2TiO_5 sintering. They found that the formation of pure AI_2TiO_5 initially occurs by a nucleation and rapid growth process and, afterward, by the slow conversion of unreacted oxides controlled by solid-state diffusion.

Different strategies have been proposed and employed for obtaining Al_2TiO_5 based materials, including the direct oxide mixture and firing, several chemical routes based on sol–gel synthesis and other chemical routes [6, 11, 16], and even other industrial by-products [19].

Although the alumina–titania system has been studied, there is still interest in the practical features for designing this family of materials, especially from commercial industrial grade starting powders, since the processing–property-behavior relations have not been completely described.

In the present work, we report a full characterization of two Al_2TiO_5 materials obtained from simple equimolar alumina–titania mixtures with different alumina particle sizes (≈ 0.5 and ≈ 2.5 μm), focusing on the dynamic thermal shrinkage behavior. The difference in the starting particle size results in different thermal behaviors and properties. This comparison will enlighten the design strategies of this kind of material.

Experimental

Material processing

Three commercial powders with industrial availability were studied. Two equimolar mixtures of α-Al_2O_3 and TiO_2 were compared. As mentioned, the alumina powders size was the principal difference. For the titanium oxide source, TiO_2 (titanium (IV) oxide, Cicarelli) with 95% anatase and 5% rutile (D_{50}: 2 μm) was chosen. Aluminum oxide: A-2G (ground, G) and A-16SG (super ground, SG) were compared; both powders are from Almatis GmbH, Germany. Aluminas properties are shown in Table 1. Samples were labeled based on the alumina employed: G-AT and SG-AT, respectively.

An initial mixture was carried out in a planetary ball mill Fritsch Pulverisette 7, with isopropyl alcohol performing 5 cycles of 2 min at 500 rpm, with 1 min of pause between cycles. The mixed slurry was dried and sieved through a 100-mesh screen. The samples were shaped by uniaxial pressing at 50 MPa. Thus, $20 \times 3 \times 3$ mm^3 prismatic probes were obtained. These probes were fired in an electric furnace with a heating rate of 5°C min^{-1} up to 1500 °C with 2 h soaking and a cooling rate of 10 °C min^{-1} down to 300 °C. The maximum temperature was chosen after a dilatometric study and taking into account previous reports [8, 9, 20].

Materials characterizations

Simultaneous thermogravimetric (TG) and differential thermal analysis (DTA) was performed on starting mixtures on Netzsch STA 409c equipment, at 10 °C min^{-1} heating rate in air atmosphere up to 1450 °C. To understand the sintering behavior, thermomechanical analysis on vertical prismatic sample ($20.0 \times 3.5 \times 3.5$ mm^3) was also performed, with a 5 °C min^{-1} heating rate in air atmosphere up to 1450 °C (TMA Rigaku Evo plus II, Japan); this has been recently carried out for ceramic based composites [21–23].

The crystalline phases of the sintered samples were determined by X-ray diffraction (XRD) using CuKα radiation operating at 40 kV and 35 mA. Materials calcined at intermediate temperatures (1150 and 1250 °C) were also studied in order to confirm the thermal processes observed in TMA.

The apparent density and open porosity of the sintered samples were evaluated by the Archimedes method in water. Mercury intrusion tests were performed by using a mercury porosimeter Thermo Scientific Pascal 440 Series [24]. The microstructure analysis was done by scanning electron microscopy (SEM) (JEOL, JCM- 6000); free fracture gold-coated surfaces were analyzed. Afterward, the dilatometric

Table 1 Mean particle size and chemical composition of alumina powders

Commercial alumina	Mean particle size D_{50}/μm	Chemical composition/mass%							
		TiO_2	Al_2O_3	Fe_2O_3	SiO_2	Na_2O	B_2O_3	MgO	CaO
A-2G	2.92[a]	–	99.6	0.02	0.03	0.25	0.01	–	–
A-16SG	0.5	–	99.8	0.02	0.03	0.07	< 0.005	0.05	0.02

[a]Queiroga JA, Nunes EHM, Souza DF, Vasconcelos DCL, Ciminelli VST, Vasconcelos WL. Microstructural investigation and performance evaluation of slip-cast alumina supports. Ceramics International. 2017; https://doi.org/10.1016/j.ceramint.2016.12.037

behavior of the completely converted material was established (Rigaku Evo II, Japan).

Flexural strength (σ_f) was measured on the bars with rectangular Section ($3.5 \times 3.5 \times 20$ mm^3) using the 3-point bending test with 15 mm of span, and a displacement rate of 0.1 mm min^{-1} was employed (universal testing machine INSTRON 5985). The dynamic elastic modulus, E, of the materials was measured by the excitation technique with a GrindoSonic, MK5 "Industrial" Model. Eight bars were evaluated for the mechanical characterizations [25].

Results and discussion

The DTA has previously shown to be adequate for evaluating Al_2TiO_5 formation from pure oxides [9]. Figure 1 shows the DTA curves of the two studied mixtures. The peak shape is Gaussian in both cases (R^2: above 0.9). The onset temperatures of endothermic peaks in both curves are 1380 and 1385 °C, respectively. The local minimum is also different: the SG-AT sample peak is centered at 1405 °C, and for the coarser alumina mixture G-AT, it is centered at a 10 °C higher temperature. Both samples finish AT formation at around 1440 °C.

The intensity of the signal is also different. The SG-AT presents a higher intensity (2.5 times higher). Evidently, there is a difference on the advance of the reaction for the different alumina powders, and the DTA test permits to observe this difference only proportionally. It is worth pointing out that for both systems, the reaction is advanced in a range of 60 °C at 10 °C min^{-1}.

Figure 2 shows the diffraction patterns of the sintered materials. They confirm Al_2TiO_5 conversion. It is complete for the SG-AT material and incomplete for the G-AT one. In the latter, alumina (Al_2O_3) and titania (TiO_2) diffraction lines accompany the Al_2TiO_5 peaks. These could be due

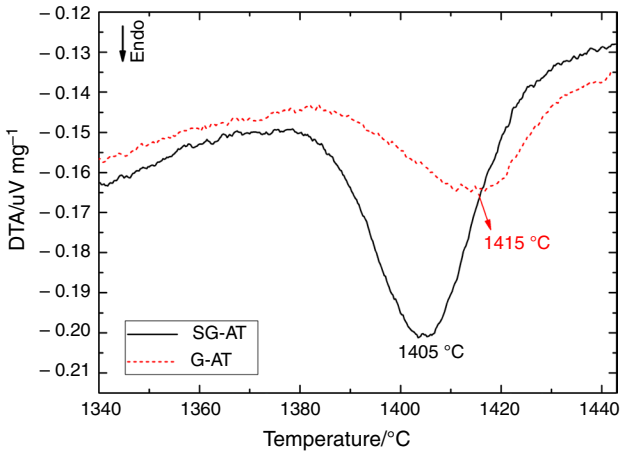

Fig. 1 DTA curves of the alumina–titania mixtures

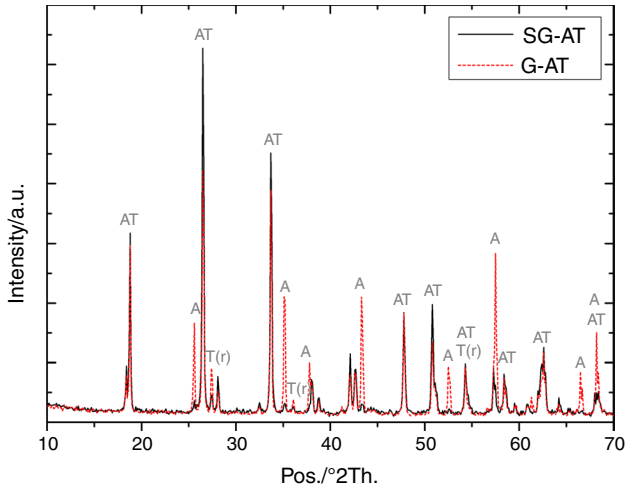

Fig. 2 XRD patterns of the sintered alumina–titania mixtures. AT: Al_2TiO_5 (PDF 00-041-0258), A: Al_2O_3 (PDF 01-083-2080), T(r): TiO_2 rutile (PDF 01-078-1509)

to a partial decomposition during cooling or because some not negligible portion of the reagents can get trapped in the AT product without a counterpart being available for AT formation [17].

Dynamic sintering characterization TMA-dTMA

The dynamic reversible sintering curves (TMA) are plotted in Fig. 3. The shrinkage–temperature behavior of the alumina–titania mixtures is complex [17]. For better visualization and to establish the limit of the thermal processes, both the $\Delta L/L\%$ curve and its derivative curve are shown in Fig. 4. The shrinkage–temperature behaviors of both samples present two sigmoidal shrinkages that start at 900 °C

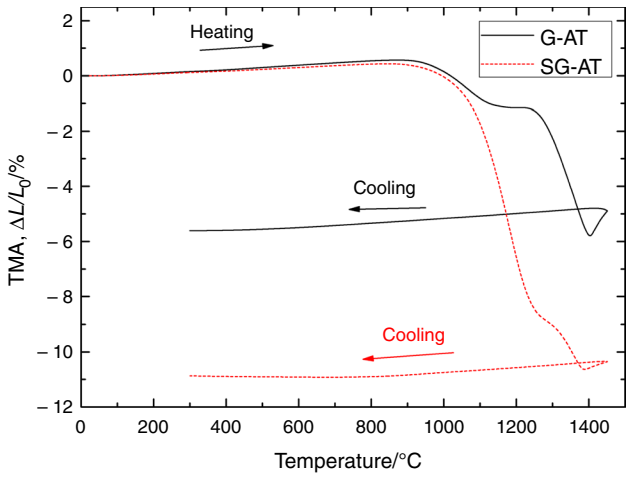

Fig. 3 Reversible sintering curves of the alumina–titania mixtures at 5 °C min^{-1}; $\Delta L/L_0$ as a function of temperature/°C

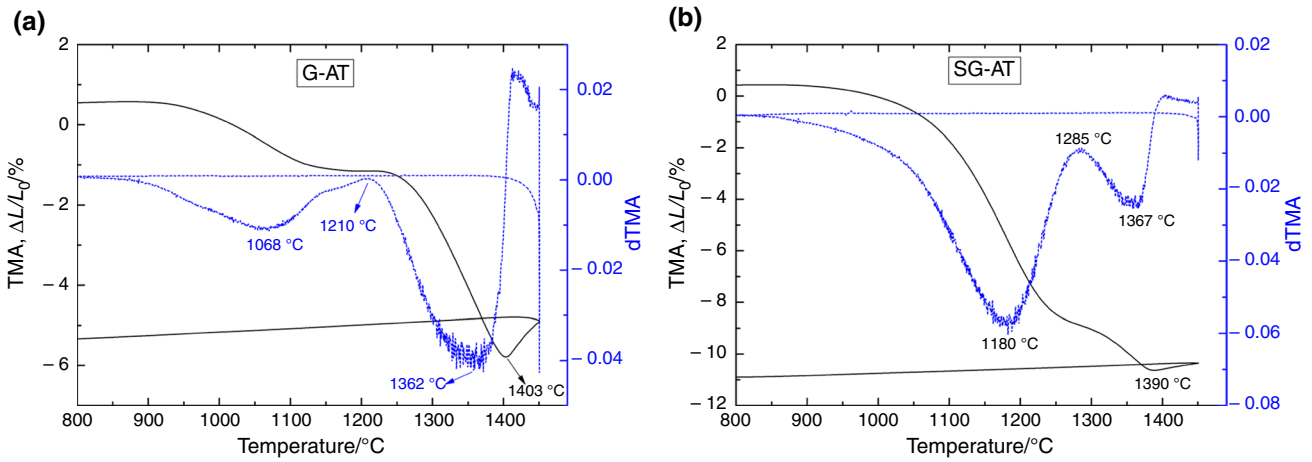

Fig. 4 Range of sintering and reaction sintering of the TMA and dTMA curves of the alumina–titania mixtures. **a** G-AT; **b** SG-AT

and finish around 1400 °C (1403 and 1390 °C for G-AT and SG-AT samples, respectively). Afterward, an expansion can be observed up to the maximum tested temperature (1450 °C). It is important to take into account that the reaction range is between 1380 and 1440 °C (DTA curve in Fig. 1), which shows that the mentioned first shrinkages occur without reaction; only the second process is overlapped with Al_2TiO_5 formation.

Figure 5 shows the XRD patterns of quenched samples after the first alumina–titania sintering stage; the final temperature was established after TMA tests (SG-AT: 1250 °C, G-AT: 1150 °C). Above this temperature, the reaction sintering (RS) processes began. Strictly, it consists of a sintering process, which could be understood as a second sintering stage of the starting powders, that starts at 1200 °C for the G-AT and 1280 °C for the SG-AT and is accompanied by the reaction above 1380 °C only. Afterward, for both samples, above 1430 °C the only thermal effect is the thermal expansion up to the final maximum temperature.

The cooling behavior presents a slight shrinkage of the developed phases. In the SG-AT material, this shrinkage is followed by a constant size stage from 700 °C to room temperature (RT). This was already observed in several Al_2TiO_5 studies [11, 12]. During the cooling cycle, the contraction is possibly accompanied by the development and closure of the typical microcracks [2, 15–17].

The two-step sintering process of the starting materials is the main difference observed. This results in a different final shrinkage, which for SG-AT powder is ≈ 12% and for G-AT half of that of the former.

In fact, the main difference is observed in the first sigmoidal shrinkage assigned to the alumina sintering (Fig. 4). Evidently, the finest SG-AT starting alumina powder presents a more important sintering, which is 2% for G-AT and around 9% for SG-AT. This first sintering stage ends at different

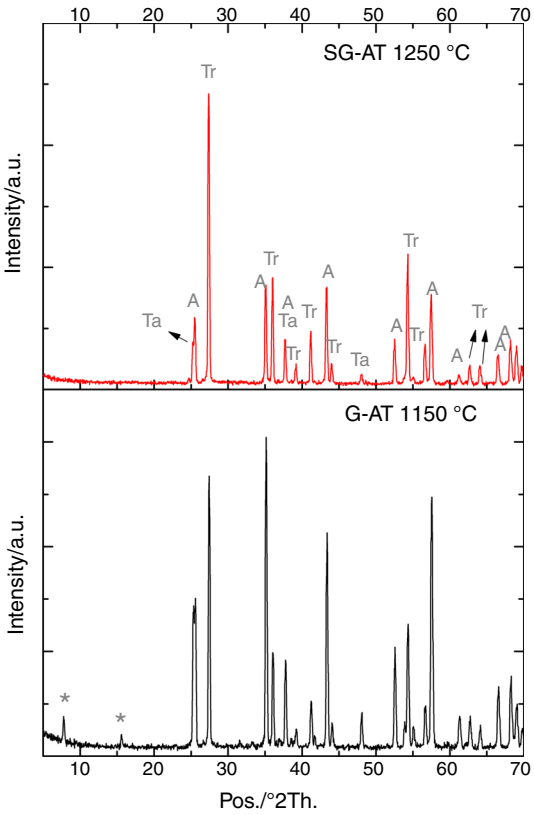

Fig. 5 XRD patterns of the alumina–titania mixtures after the first sintering stage. AT: Al_2TiO_5 (PDF 00-041-0258), A: Al_2O_3 (PDF 01-083-2080), T(r): TiO_2 rutile (PDF 01-078-1509), T(a): TiO_2 anatase (PDF 01-078-2486), *: $NaAl_{11}O_{17}$ diaoyudaoite (PDF 01-079-2288)

temperatures also: 1150 °C and 1285 °C for the G-AT and SG-AT respectively. After this multitechnique approach, the complete thermal cycle was studied in a reversible way. The whole thermochemical processes are listed in Table 2.

Table 2 Initial and final temperatures of the thermochemical processes of the alumina–titania mixtures

Stage	Processes	Initial Temp./°C	Final Temp./°C	G-AT		SG-AT	
				Initial $\Delta L/L_0$/%	Final $\Delta L/L_0$/%	Initial $\Delta L/L_0$/%	Final $\Delta L/L_0$/%
1	Reagent (alumina and titania) thermal expansion	RT	900	0	0.5	0	0.5
2	Starting powders sintering, first stage.	900	1150 (G-AT) 1280 (SG-AT)	0.5	−1.5	0.5	−9.5
3	Starting powders sintering, second stage.	1200 (G-AT) 1280 (SG-AT)	1400	−1.5	−6.5	−9.5	−11.0
4	Al_2TiO_5 formation (from DTA)	1380 (SG-AT) 1385(G-AT)	1440	Not applicable			
5	Al_2TiO_5 thermal expansion up to final temperature	1400	1450	−6	−5.0	−11.5	−10.5
6	Al_2TiO_5 shrinkage during cooling	1450	700	−5.0	−5.5	−10.5	−11.0
7	Al_2TiO_5 final cooling down to room temperature	700	RT	−5.5	−5.5	−11.0	−11.0

Table 3 Textural properties of the sintered alumina–titania mixtures

Sample	Immersion test		Hg Porosimetry		
	Apparent density/ gcm^{-3}	Open porosity/ %	D_{10}/μm	D_{50}/μm	D_{90}/μm
G-AT	2.56 ± 0.04	27.7 ± 0.1	3.0	2.0	1.2
SG-AT	3.02 ± 0.03	12.5 ± 0.2	2.1	1.0	0.2

This is more detailed if compared with Buscaglia et al. [18] description. The finer the alumina the faster the sintering of the starting powders previous to Al_2TiO_5 formation, with the expectable corresponding differences in the developed microstructure.

Textural properties and microstructure

The analysis consisted of the immersion test, the mercury intrusion test, and microstructural characterization by SEM. Table 3 lists the immersion test results, showing an important difference in the achieved porosities and densities. While the achieved density of the SG-AT material is higher than that of G-AT, the resulting porosity of G-AT doubles that of the SAG-T mixture. In both cases, the achieved densification is low, as was previously observed [11, 12, 18]. A complete densification would require a different processing route. Perhaps a first formation step followed by a sinterization would be a better route for this purpose [15].

Different pore size distributions were achieved (see Table 3). Both materials presented fine microstructures with pores below 4 μm. As expected, the D_{50} values of G-AT double the D_{50} of the SG-AT material. The SG-AT material presented an important volume fraction of pores below 0.5 μm.

Figure 6 shows SEM images of the G-AT and the SG-AT free fractures. The developed microstructures are comparable to the ones described elsewhere [6, 11, 12, 15]. Particularly, in both materials a homogenous grain size distribution can be observed. Rounded Al_2TiO_5 grains are observed. The higher sinterization of the SG-AT material is evident. In the G-AT material, the interstitial porosity is visible (darker gray). The crack presence is clear in both samples, but the higher sintering of SG-AT permits a better observation.

The grain size distribution is difficult to evaluate from the SEM images. Roughly, the grain size of SG-AT material is around 1–5 μm, although it presents some bigger sintered grains. On the other hand, the grain sizes for G-AT are noticeably wider; small grains (1–3 μm) can be observed together with other bigger grains up to 5–7 μm. With this analysis, no further differentiation of the developed microstructures can be carried out. However, the difference would be more evident in the mechanical and thermomechanical characterization of the samples at a macroscopic level, as is shown in the following sections.

Mechanical properties and thermal expansion behavior

It is known that the mechanical behavior of a ceramic material is related to its microstructural features. Particularly, this is affected (lowered) by the presence of pores and or cracks [2, 16, 26]. The achieved flexural strengths are around the reported values [11, 17] for undoped Al_2TiO_5 materials (Table 4). The evaluated relative dispersion is slightly high, but this fact is expectable for these cracked microstructures. The evaluated dynamic stiffness is also low and remarkably similar; apparently, the combination of both porosity and crack effects is similar for the two materials. The observed dispersion in the dynamic stiffness is good and

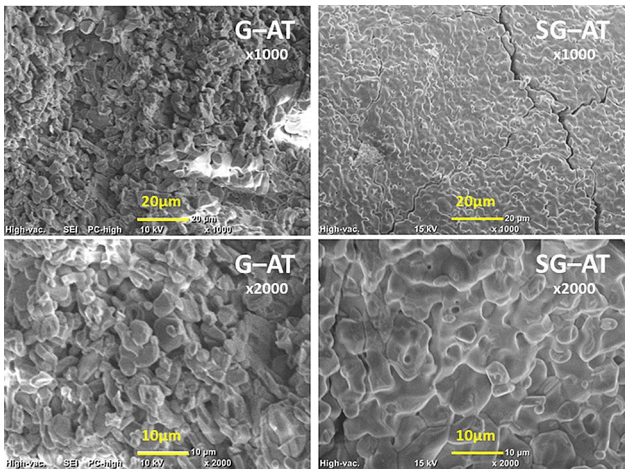

Fig. 6 SEM images (x1000 and x2000) of the developed Al_2TiO_5 materials

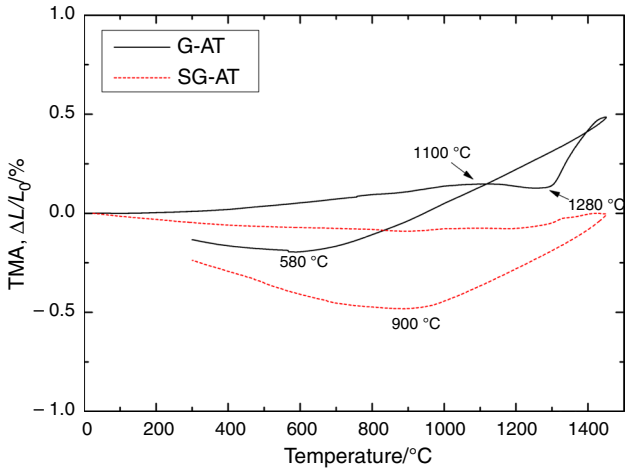

Fig. 7 Complete reversible dilatometric curve of the sintered Al_2TiO_5 materials

Table 4 Flexural strength (σ_f), dynamic elastic modulus (E_d) and thermal expansion coefficient ($\alpha_{25-1000\ °C}$) of the sintered materials

Sample	σ_f/MPa	E_d/GPa	$\alpha_{25-1000\ °C}/\times 10^{-6}\ °C^{-1}$
G-AT	5.2 ± 1.2	5.8 ± 0.3	0.014
SG-AT	5.5 ± 1.8	5.5 ± 1.1	− 0.872

is a consequence of the global behavior characterization of this method. On the other hand, the 3-point bending test is strongly affected by the particular presence and distribution of defects in the center of prismatic samples [27, 28].

As mentioned, the low thermal expansion of the Al_2TiO_5 based materials is one of their distinctive characteristics [6–8, 11, 15, 17]. The values of the thermal expansion coefficients are shown in Table 4 in the technological temperature range (below 1000 °C). Both materials present remarkably low thermal expansion coefficients; in fact, the SG-AT material presents a negative value in the 0–800 °C range. This encourages the use of these materials in severe thermomechanical applications [6, 7]. However, the titanate chemical stabilization must be performed if high temperature applications are intended, due to the thermal instability of Al_2TiO_5 [6, 11, 15].

The actual expansion behavior would be related, for example, to the particular anisotropic crystal thermal expansion, the presence of pores, and developed cracks. At this point, it is not easy to establish a direct relation between the described microstructural features and this difference in the expansion behavior. The higher sinterization grade of the SG-AT material leads to higher crack development, which close during subsequent heating of the materials. This local crack closure results in a macroscopic low or even negative thermal expansion coefficient [2, 16].

The observed hysteresis in the complete dilatometry (Fig. 7) of the fired samples presents the typical hysteresis behavior and is a consequence of the anisotropic thermal expansion of the Al_2TiO_5 grains, and the crack matrix developed during the reaction sintering process [7, 16]. This is also similar to the ones observed in similar materials [2, 4, 6, 7, 16]. However, it could be said that the observed differences evidence the difference in the crack matrix, showing the effect of the starting powder on the developed microstructure.

Conclusions

- Aluminum titanate materials were successfully processed from different fine commercial powders and characterized. Particularly, two calcined aluminas were compared through a multitechnique approach. This allowed the description of all the thermochemical processes during thermal treatment. An incomplete sintering was observed, which is expectable for this system.
- Developed phases were established; ceramics with complex microstructures were obtained and described. They presented interlocked grains and an interconnected microcrack matrix that do not jeopardize the material integrity.
- The lower alumina particle size enhances the sintering and reaction advance processes. The thermal treatment was optimized. The sintering process of the unreacted reagents (alumina and titania) was described (between 900 and ≈ 1250 °C). This is the main difference observed

between samples and becomes more important with the finer alumina.

- In both mixtures, a two-step sintering process was observed. The second process is partially overlapped with a reaction (Al_2TiO_5 formation) process. These were delimited after the performed analysis, demonstrating the adequacy of the employed thermal techniques.
- In the technological range (RT-1000 °C), low or slightly negative thermal expansion coefficients were observed. This, together with the mechanical behavior, encourages structural applications with high thermomechanical solicitations of Al_2TiO_5 based materials.

Acknowledgements MAV and MFH acknowledge CONICET for the fellowships; this work was partially financed by ANPCyT (PICT-2016-1193) and CONICET (PIO CONICET-UNLA 2016-2018. No. 22420160100023), and UNLP (2015-2018 X-737). MSC is member of the CIC-PBA; GS and NMR are members of the CONICET.

References

1. Bakhshandeh F, Azarniya A, Madaah H, Jafari S. Are aluminium titanate-based nanostructures new photocatalytic materials? Possibilities and perspectives. J Photochem Photobiol A. 2018. https://doi.org/10.1016/j.jphotochem.2017.11.043.
2. Ohya Y, Nakagawa Z. Measurement of crack volume due to thermal expansion anisotropy in aluminium titanate ceramics. J Mater Sci. 1996. https://doi.org/10.1007/BF00357864.
3. Thomas HAJ, Stevens R. Aluminium titanate—a literature review. Part 2. Engineering properties and thermal stability. Br Ceram Trans J. 1989;88:184–90.
4. Thomas HAJ, Stevens R. Aluminium titanate—a literature review. Part 1. Microcracking phenomena. Br Ceram Trans J. 1989;88:144–51.
5. Giordano L, Viviani M, Bottino C, Buscaglia MT, Buscaglia V, Nanni P. Microstructure and thermal expansion of Al_2TiO_5–$MgTi_2O_5$ solid solutions obtained by reaction sintering. J Eur Ceram Soc. 2002. https://doi.org/10.1016/S0955-2219(01)00503-9.
6. Kim IJ. Thermal stability of Al_2TiO_5 ceramics for new diesel particulate filter applications-a literature review. J Ceram Process Res. 2010;11:411–8.
7. Kim IJ. Thermal shock resistance and thermal expansion behavior of Al_2TiO_5 ceramics prepared from electrofused powders. J Ceram Process Res. 2000;1:57–63.
8. Violini MA, Hernández MF, Gauna M, Suarez G, Conconi MS, Rendtorff NM. Low (and negative) thermal expansion Al_2TiO_5 materials and Al_2TiO_5–$3Al_2O_3{\cdot}2SiO_2$–$ZrTiO_4$ composite materials. Processing, initial zircon proportion effect, and properties. Ceram Int. 2018. https://doi.org/10.1016/j.ceramint.2018.08.208.
9. Rendtorff NM, Suárez G, Aglietti EF. Non isothermal kinetic study of the aluminium titanate formation in alumina–titania mixtures. Ceramica. 2014. https://doi.org/10.1590/S0366-69132014000300013.
10. Parker FJ. Al_2TiO_5–$ZrTiO_4$–ZrO_2 composites: a new family of low-thermal-expansion ceramics. J Am Ceram Soc. 1990. https://doi.org/10.1111/j.1151-2916.1990.tb05138.x.
11. Nagano M, Nagashima S, Maeda H, Kato A. Sintering behavior of Al_2TiO_5 base ceramics and their thermal properties. Ceram Int. 1999. https://doi.org/10.1016/S0272-8842(98)00083-2.
12. Tsetsekou A. A comparison study of tialite ceramics doped with various materials and tialite–mullite composites: microstructural, thermal and mechanical properties. J Eur Ceram Soc. 2005. https://doi.org/10.1016/j.jeurceramsoc.2004.03.024.
13. Fukuda M, Yokoo T, Takahashi M. Effect of SiO_2 addition on thermal properties of Al_2TiO_3 ceramics. J Soc Mater Sci Jpn. 2015. https://doi.org/10.2472/jsms.64.609.
14. Barrios de Arenas I. Reactive sintering of aluminum titanate. In: Lakshmanan A, editor. Sintering of ceramics—new emerging techniques. Croatia: InTech; 2012. pp. 501–28.
15. Baudín de la Lastra C, Uribe R. Formación de titanato de aluminio por reacción en estado sólido de alumina y titania. Boletín de la Sociedad Española de Cerámica y Vidrio. 2000; https://doi.org/10.13039/501100007273.
16. Kim HC, Lee KS, Kweon OS, Aneziris CG, Kim IJ. Crack healing, reopening and thermal expansion behavior of Al_2TiO_5 ceramics at high temperature. J Eur Ceram Soc. 2007. https://doi.org/10.1016/j.jeurceramsoc.2006.04.024.
17. Buscaglia V, Nanni P, Battilana G, Aliprandi G, Carry C. Reaction sintering of aluminium titanate: I—effect of MgO addition. J Eur Ceram Soc. 1994. https://doi.org/10.1016/0955-2219(94)90018-3.
18. Buscaglia V, Nanni P, Battilana G, Aliprandi G, Carry C. Reaction sintering of aluminium titanate: II-effect of different alumina powders. J Eur Ceram Soc. 1994. https://doi.org/10.1016/0955-2219(94)90019-1.
19. Ewais EMM, Besisa NHA, Ahmed A. Aluminum titanate based ceramics from aluminum sludge waste. Ceram Int. 2017. https://doi.org/10.1016/j.ceramint.2017.05.057.
20. Melo MF, Moya JS, Pena P, De Asa S. Multicomponent toughened ceramic materials obtained by reaction sintering—part 3 system ZrO_2–Al_2O_3–SiO_2–TiO_2. J Mater Sci. 1985. https://doi.org/10.1007/BF00553032.
21. Łada P, Miazga A, Konopka K, Szafran M. Sintering behavior and thermal expansion of zirconia–titanium composites. J Therm Anal Calorim. 2018. https://doi.org/10.1007/s10973-017-6817-z.
22. Gizowska A, Perkowski K, Piątek M, Konopka G, Witosławska I, Tymowicz-Grzyb P. Investigation of YAP/YAG powder sintering behavior using advanced thermal techniques. J Therm Anal Calorim. 2019. https://doi.org/10.1007/s10973-019-08598-7.
23. Lu J, Li Y, Zou C, Liu Z, Wang C. Effect of heating rate on the sinterability, crystallization, and mechanical properties of sintered glass–ceramics from granite waste. J Therm Anal Calorim. 2019. https://doi.org/10.1007/s10973-018-7346-0.
24. Rendtorff N, Aglietti E. Mechanical and thermal shock behavior of refractory materials for glass feeders. Mater Sci Eng, A. 2010. https://doi.org/10.1016/j.msea.2010.02.053.
25. Roebben G, Bollen B, Brebels A, Van H, Van DB. Impulse excitation apparatus to measure resonant frequencies, elastic moduli, and internal friction at room and high temperature. Rev Sci Instrum. 1997. https://doi.org/10.1063/1.1148422.
26. Kachanov M. Elastic solids with many cracks and related problems. Adv Appl Mech. 1993. https://doi.org/10.1016/S0065-2156(08)70176-5.
27. Evans AG, Wiederhorn SM. Proof testing of ceramic materials—an analytical basis for failure prediction. Int J Fract. 1974. https://doi.org/10.1007/BF00035499.
28. Tinschert J, Zwez D, Marx R, Anusavice KJ. Structural reliability of alumina-, feldspar-, leucite-, mica- and zirconia-based ceramics. J Dent. 2000. https://doi.org/10.1016/S0300-5712(00)00030-0.